Supporting Information: Boundary Layer Dynamics after Rain Fronts: High-Resolution Reconstruction and Model Validation using ground- and drone-based Measurements

Lasse Moormann[1], Friederike Fachinger[1], Frank Drewnick[1], Holger Tost[2]

[1]Multiphase Chemistry Department, Max Planck Institute for Chemistry, Mainz, 55128, Germany
[2]Institute for Atmospheric Physics, Johannes Gutenberg University, Mainz, 55128, Germany

Correspondence to: Holger Tost (tosth@unimainz.de)

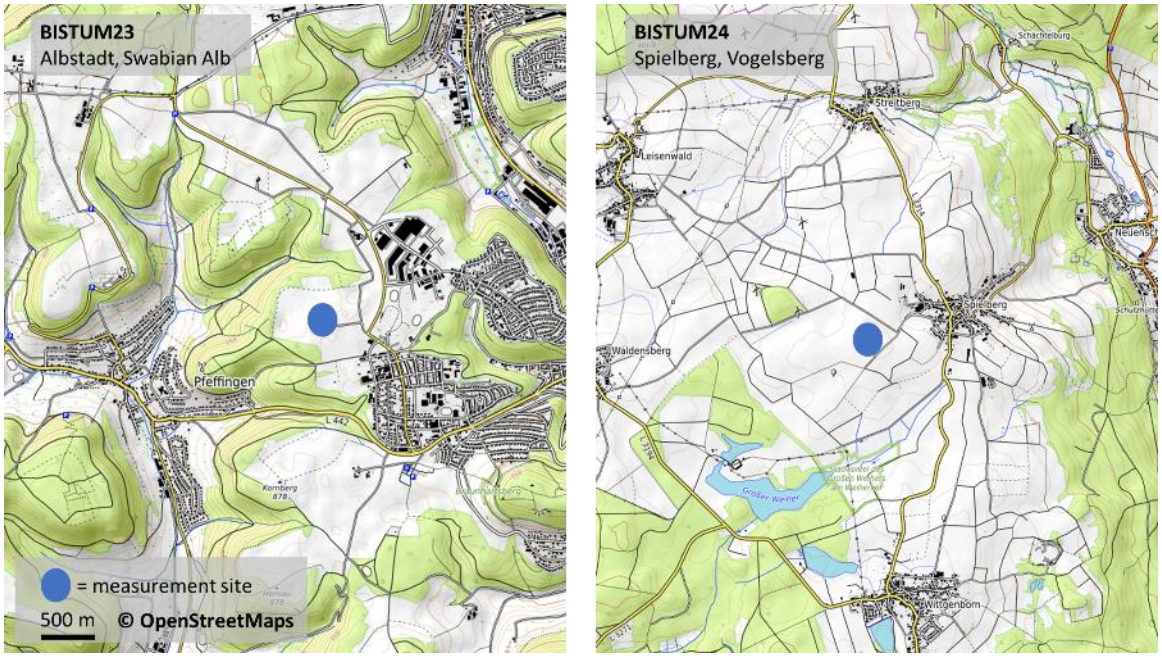

Figure S1: Topographic map of the rural measurement sites during BISTUM23 (Sect. 4) and BISTUM24 (Sect. 3) © OpenStreetMap contributors 2025. Distributed under the Open Data Commons Open Database License (ODbL) v1.0.

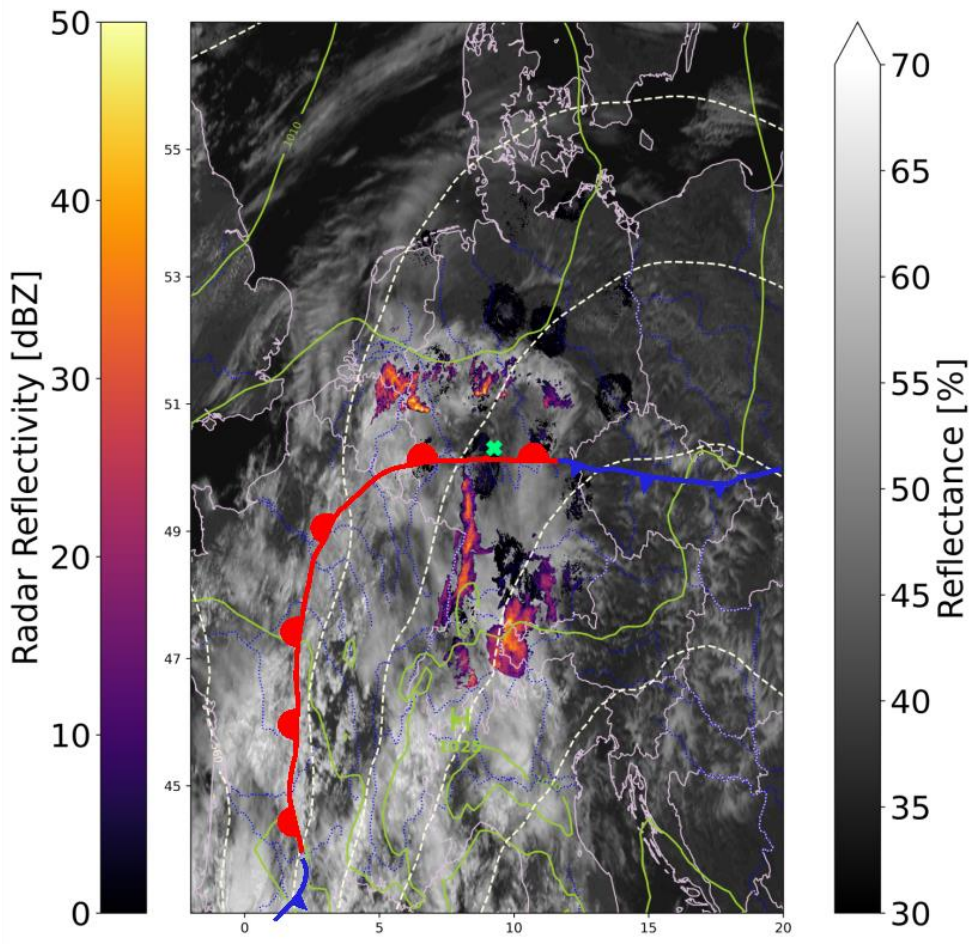

Figure S2: Synoptic map for 12:00 on 20 June 2024 including the radar reflectivity shows the measurement site (green) in a large high-pressure system close to a warm front (in red).

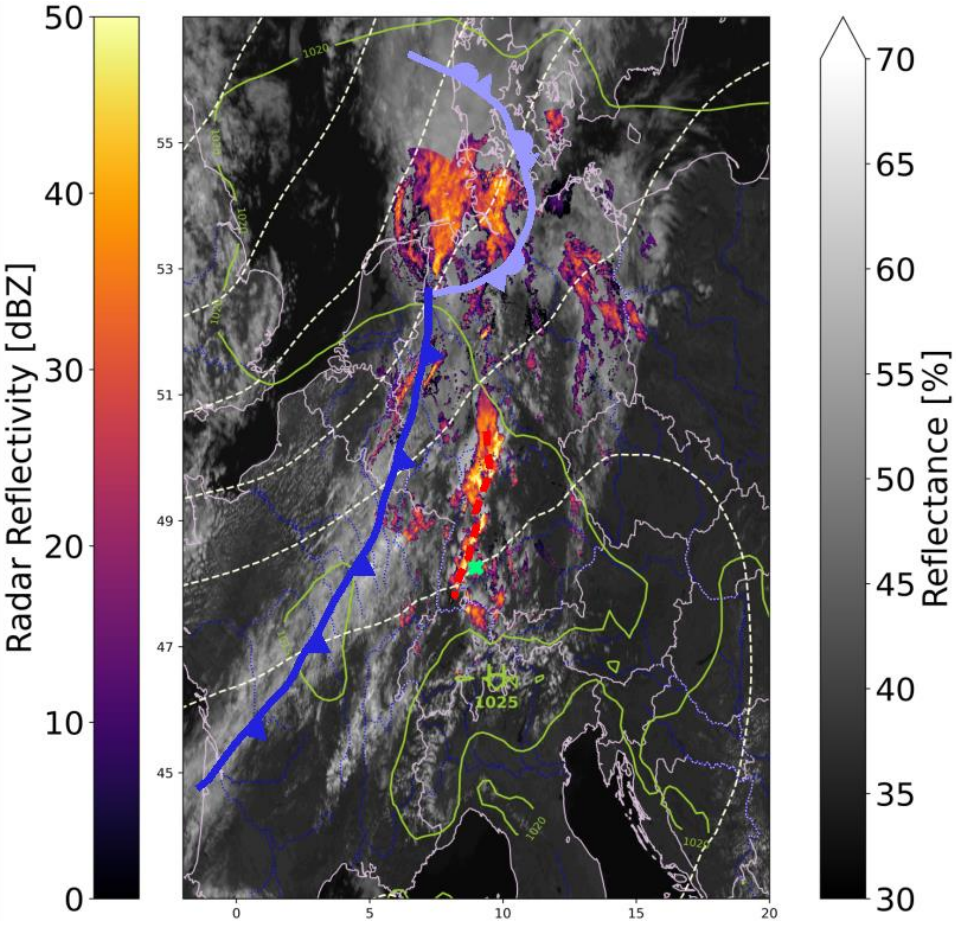

Figure S3: Synoptic map from 12:00 on 12 August 2023 including the radar reflectivity shows a convergence line (red) at the measurement site (green) in vicinity to a large cold front (blue).

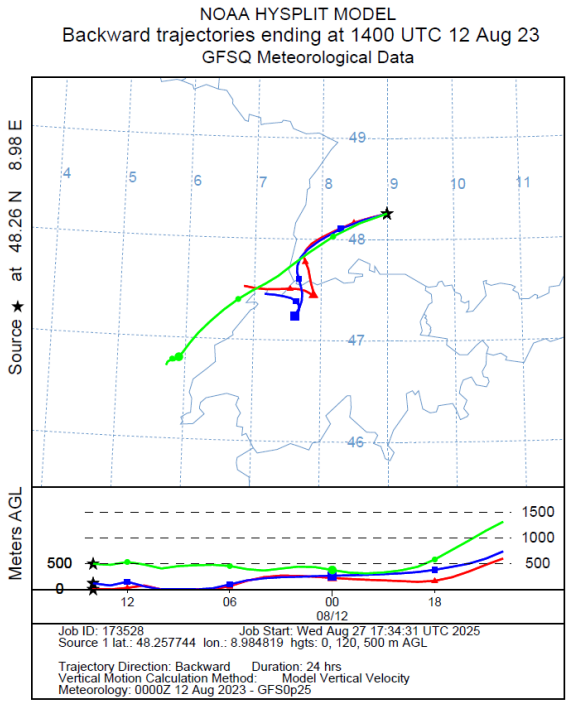

Figure S4: 24 h-backward-trajectories reaching the measurement site at 12:00 local time on 12 August 2023 reveal south-westerly aspiration from rural areas. The trajectories were calculated with the HySplit analysis tool and were started from 0 m, 120 m and 500 m above ground level (Stein et al., 2015). The near surface trajectories are influenced stronger by the underlying surface, leading to a more westerly flow at the Northern flank of the high-pressure system ~18 h before arrival, but are then partially deflected by the Alps and additionally get further into the influence of the cyclonic system over the British islands. The trajectory at elevated altitude is able to follow the free tropospheric flow more closely, such that the eastward flow, which is more driven by the free tropospheric wave pattern is less dominant.

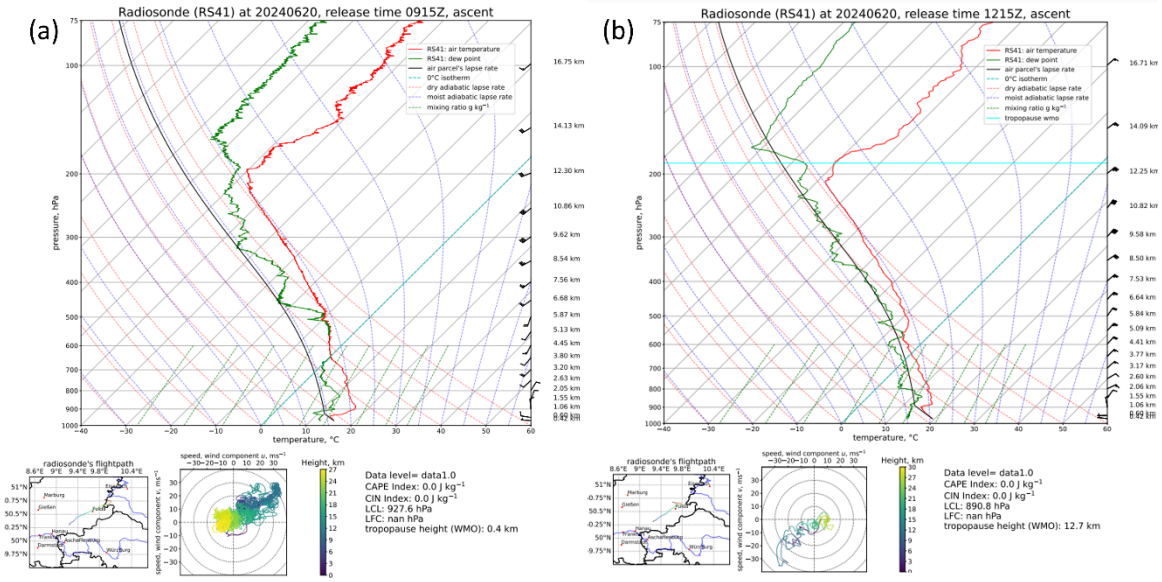

Figure S5: Radiosonde ascents on 20 June 2024 indicate stable pre- and post-rain conditions ((a) at 09:15 and (b) at 12:15).

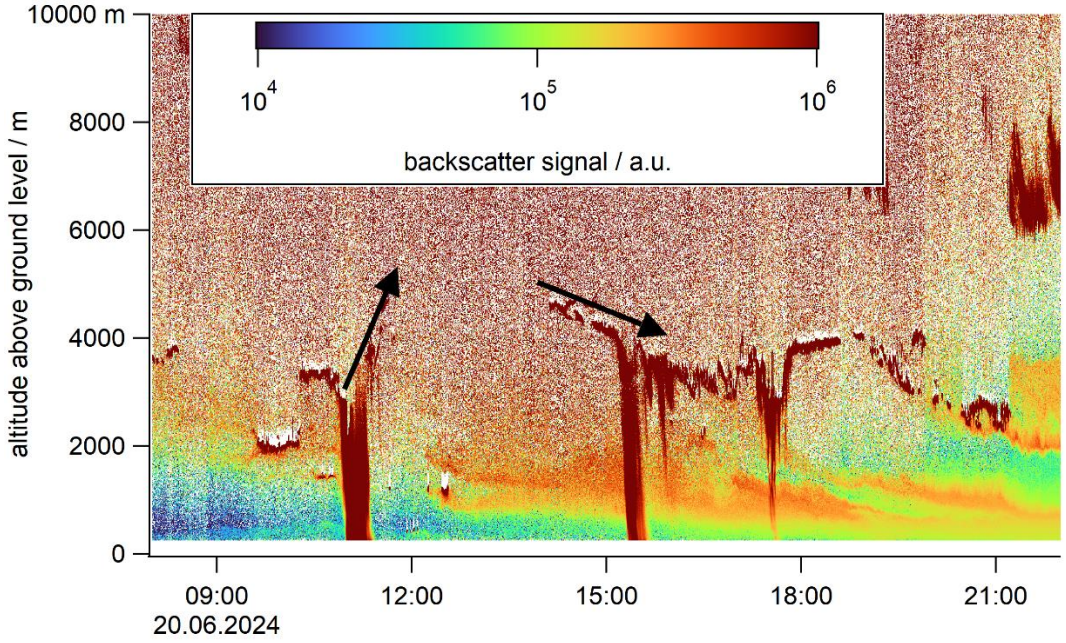

30

Figure S6: The ceilometer in MoLa monitors an uplift of clouds (dark red) from 3 km to 5 km immediately after the rainfall at 11:00 and a later decrease of layers before the second rainfall (red color reaching ground level indicates precipitation). Data of the lowermost 200 m were removed due to high uncertainties.

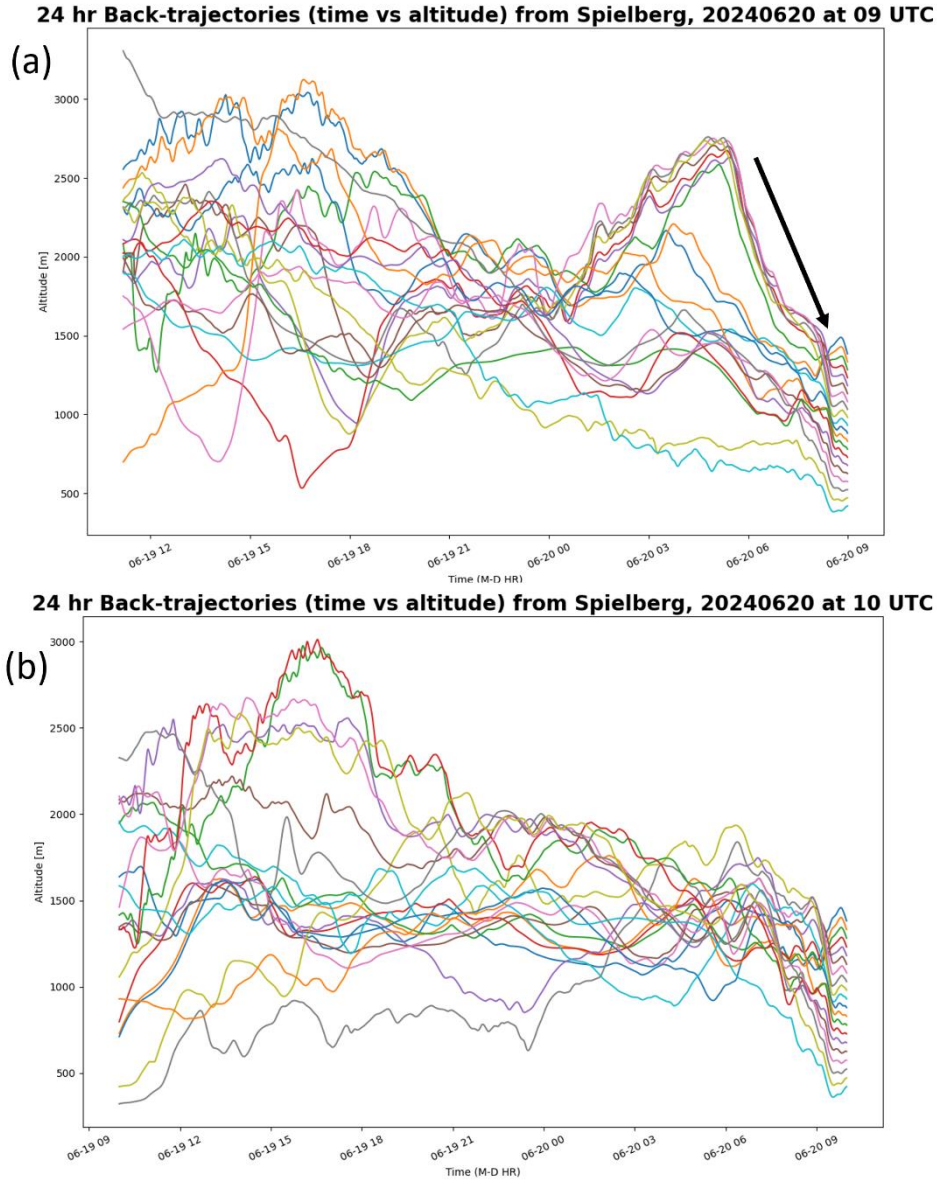

Figure S7: During the rain event, 24-h backward trajectories show a strong downdraft from 3000 m a.s.l. from 6 h before reaching the measurement site for arrival altitude levels down to 150 m a.g.l., whereas the ground-near trajectories are isolated and do not reveal strong vertical movement (a). After the rain event, the aspiration level is more than 1000 m lower and trajectories are homogenously distributed (b). Note that altitude levels are denoted as above mean sea level, and the measurement location is at 391 m a.s.l.

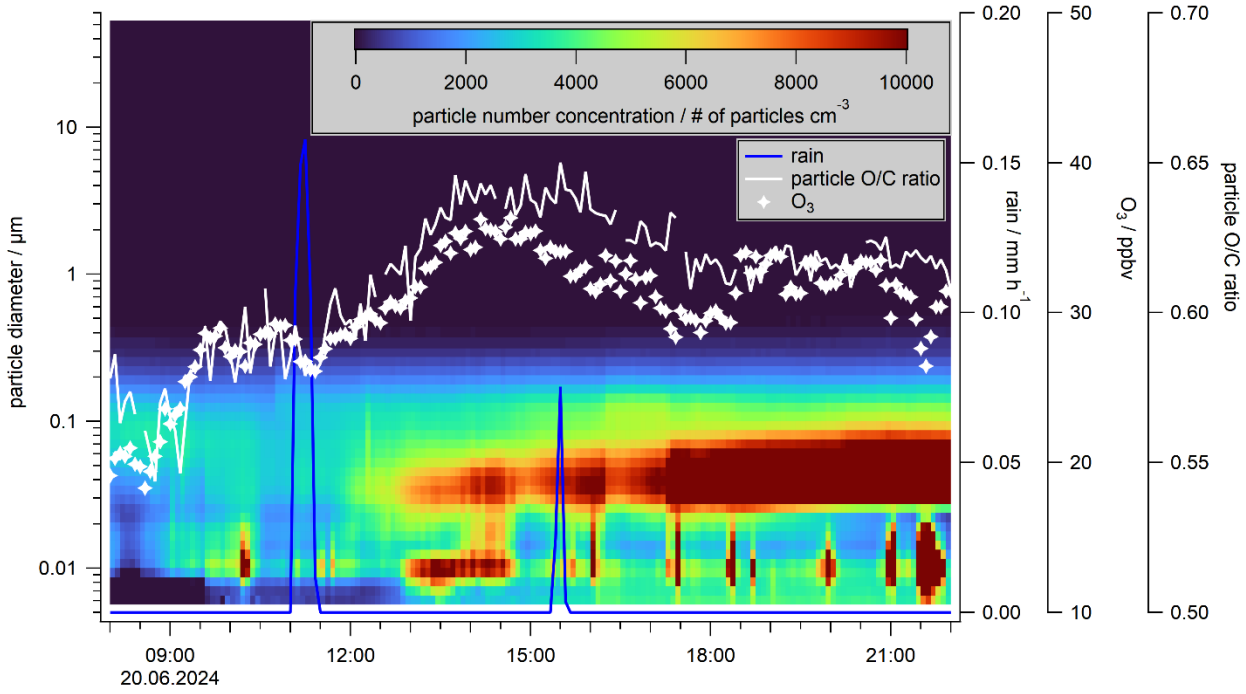

Figure S8: The good agreement of time series of O_3 (white stars) and the O/C ratio of organic particle components (white trace) measured at ground level in MoLa show an increase of oxidized aerosol particles along with oxidizing reagent. Therefore, particles form and grow as indicated by increasing mode sizes of the particle number concentration for the nucleation and Aitken mode (image plot) after the rain at 11:00 (blue).

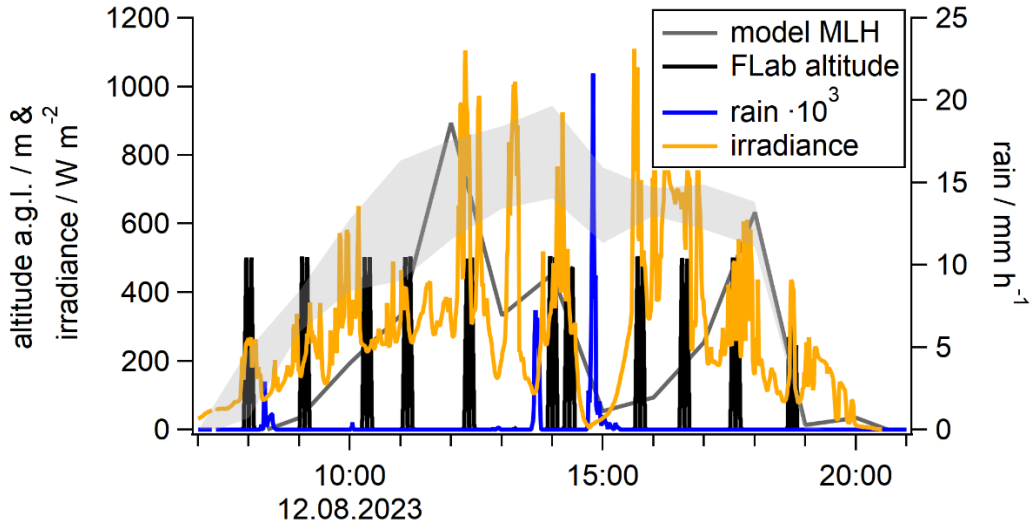

Figure S9: Time series of irradiance (orange), precipitation (blue, both 1 min averages), and the modelled MLH (grey, hourly averages) on 12 August 2023. The flight altitude of FLab is displayed in black. The shaded area represents the typical diurnal cycle of the modelled MLH at the BISTUM23 measurement site for cloudless days.

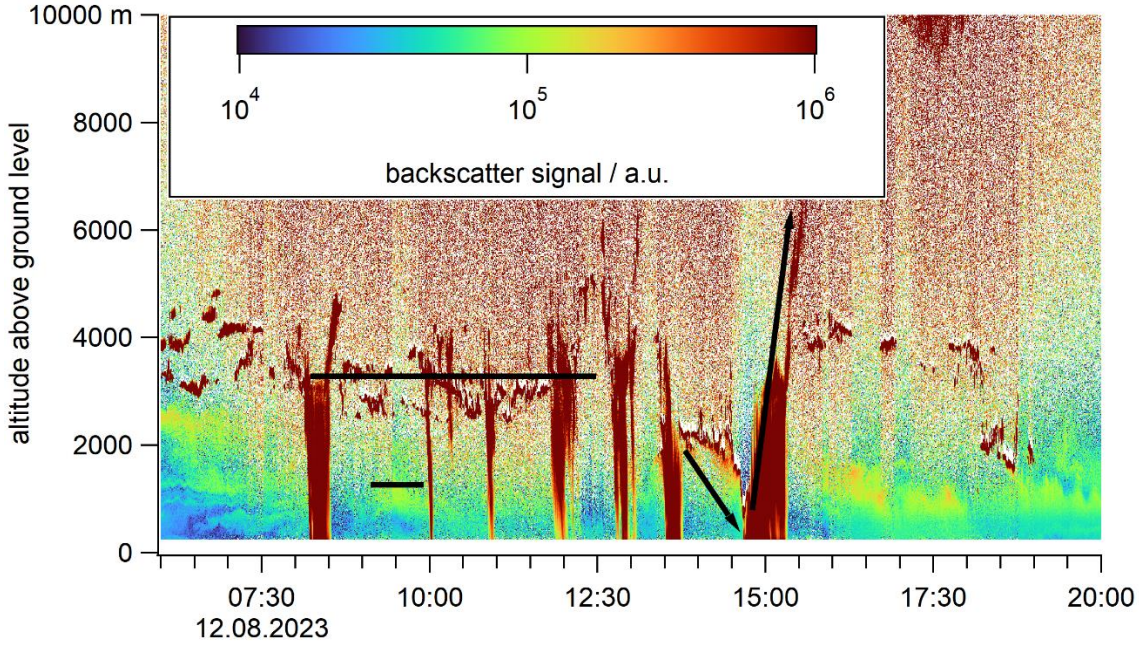

Figure S10: The ceilometer in MoLa monitors a stable cloud layer between 3 to 4 km altitude a.g.l. and frequent rain events throughout the day (indicated by dark-red color). Before the thunderstorm at 14:30, a decreased cloud layer down to 1 km a.g.l. is observed, followed by a quick increase to 7 km. Data of the lowermost 200 m were removed due to high uncertainties.

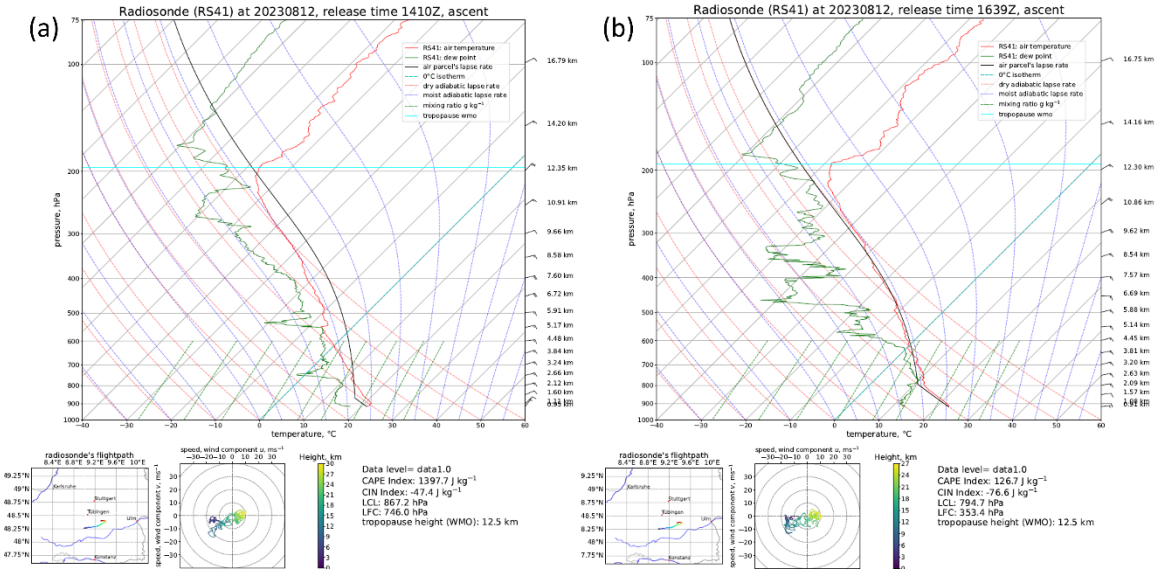

Figure S11: Radiosonde ascents on 12 August 2023 show the unstable accumulation of *CAPE* before rain ((a), 14:10) and release of *CAPE* afterwards ((b), 16:39). Altitude is given in km a.s.l.

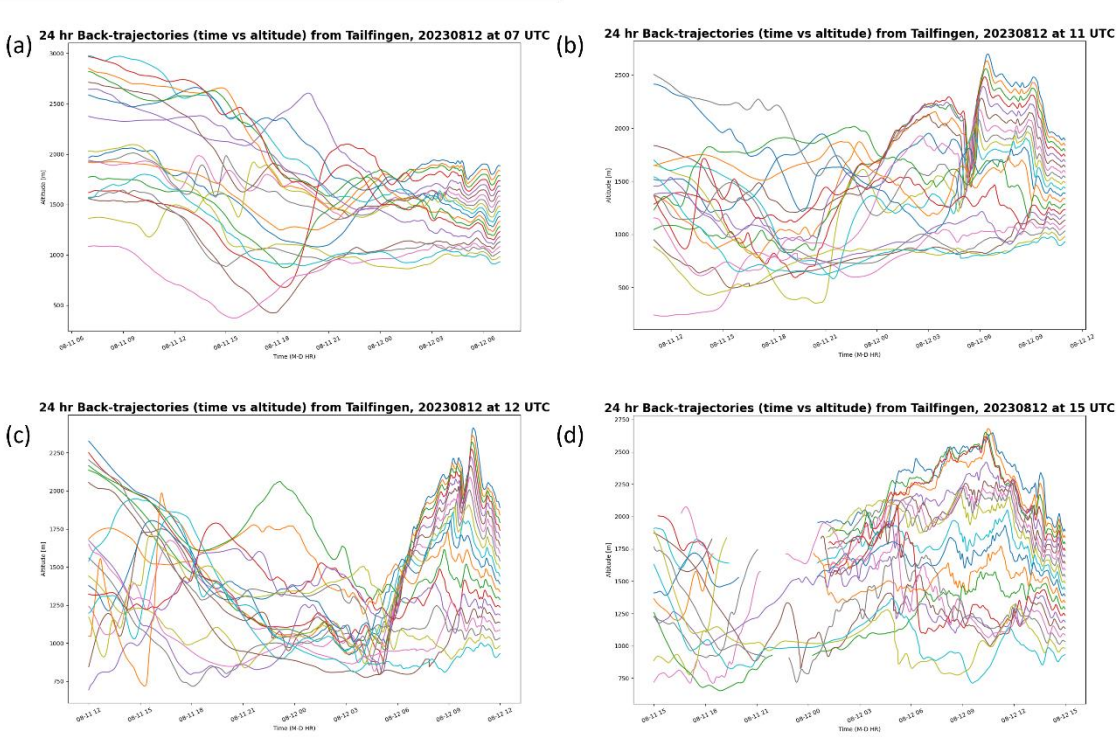

Figure 12: 24-h backward trajectories for the BISTUM23 measurement site show a shallow aspiration height in (a) at 09:00 between the first and second rain event. A strong updraft, followed by a downdraft movement were found for 13:00 and 14:00 (before the third (b) and fourth rain event (c)), whereas after the thunderstorm trajectories at 17:00 show a low downdraft, with rather parallel trajectories (d). Note the different scaling of the y-axes; altitudes shown are in m a.s.l., the measurement site was located at 886 m a.s.l. LT (local time) is given in UTC + 2 h.

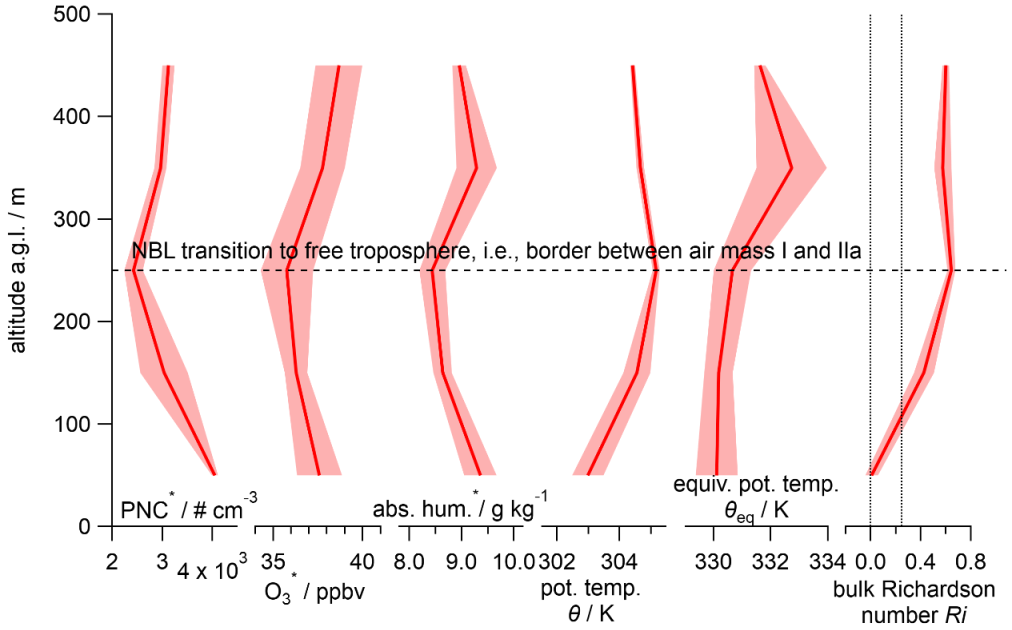

Figure S13: Medians of vertical profiles (100 m altitude increments) of the particle number concentration (PNC), O_3 mixing ratio, absolute humidity, potential temperature θ, equivalent potential temperature θ_{eq} and the bulk Richardson number *Ri* on 12 August 2023 at 08:00. Variables marked with * are corrected for temporal variation over the measurement period using the corresponding MoLa data. Error ranges represent the standard error. Dotted vertical lines indicate *Ri* = 0 and *Ri* = 0.25.

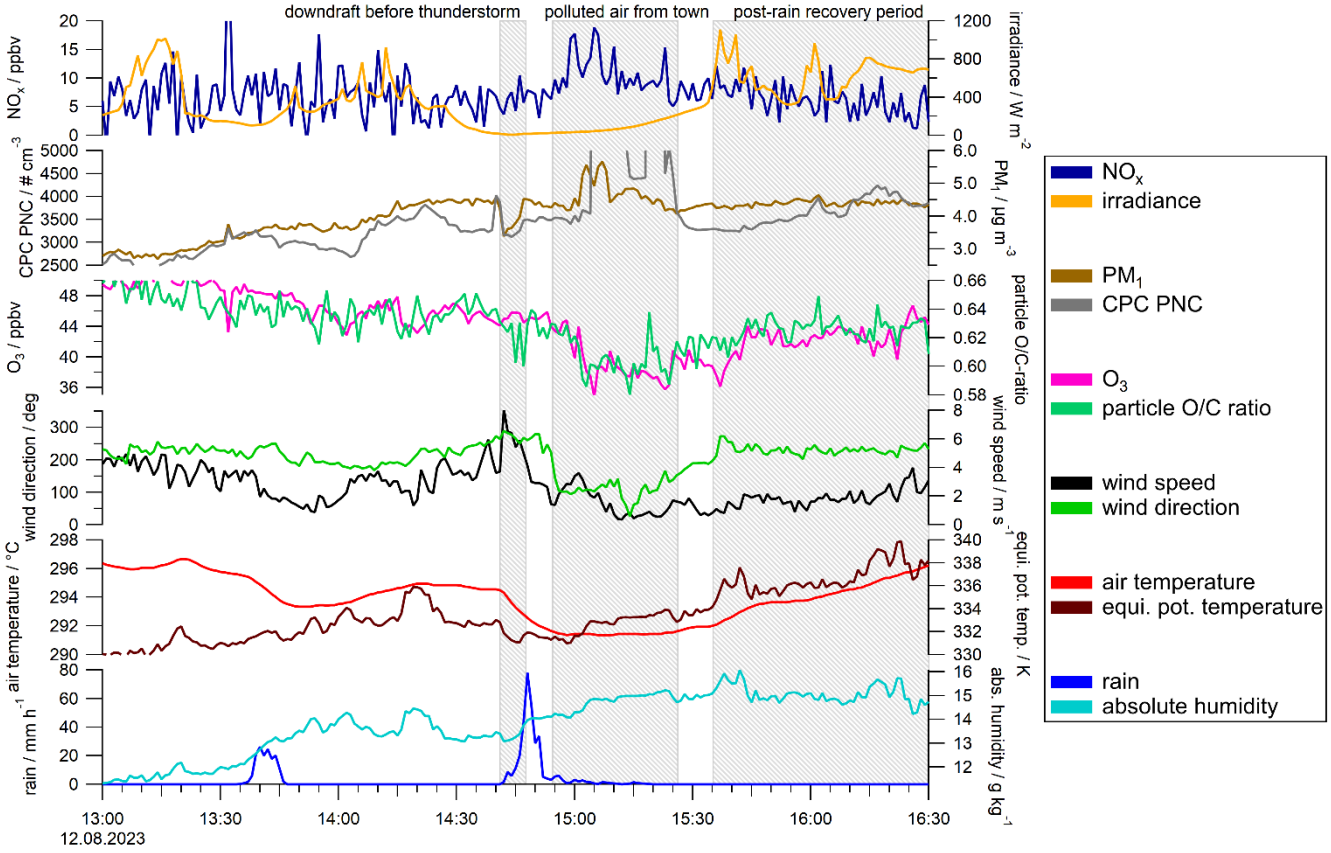

Figure S14: 1 minute-time series of PM_1 (light brown), and wind speed (dark green), measured on-board MoLa, show clean air advection before rainfall (blue). After the thunderstorm, the wind direction changes (light green) affecting measured NO_x (dark blue), particle number concentration (PNC, grey), O_3 (pink) and the O/C ratio of PM_1 organics (green). As the irradiance (yellow) increases, the absolute humidity (turquoise) also increases due to evaporation of water from ground. Descriptions of various periods are given above the shaded areas.

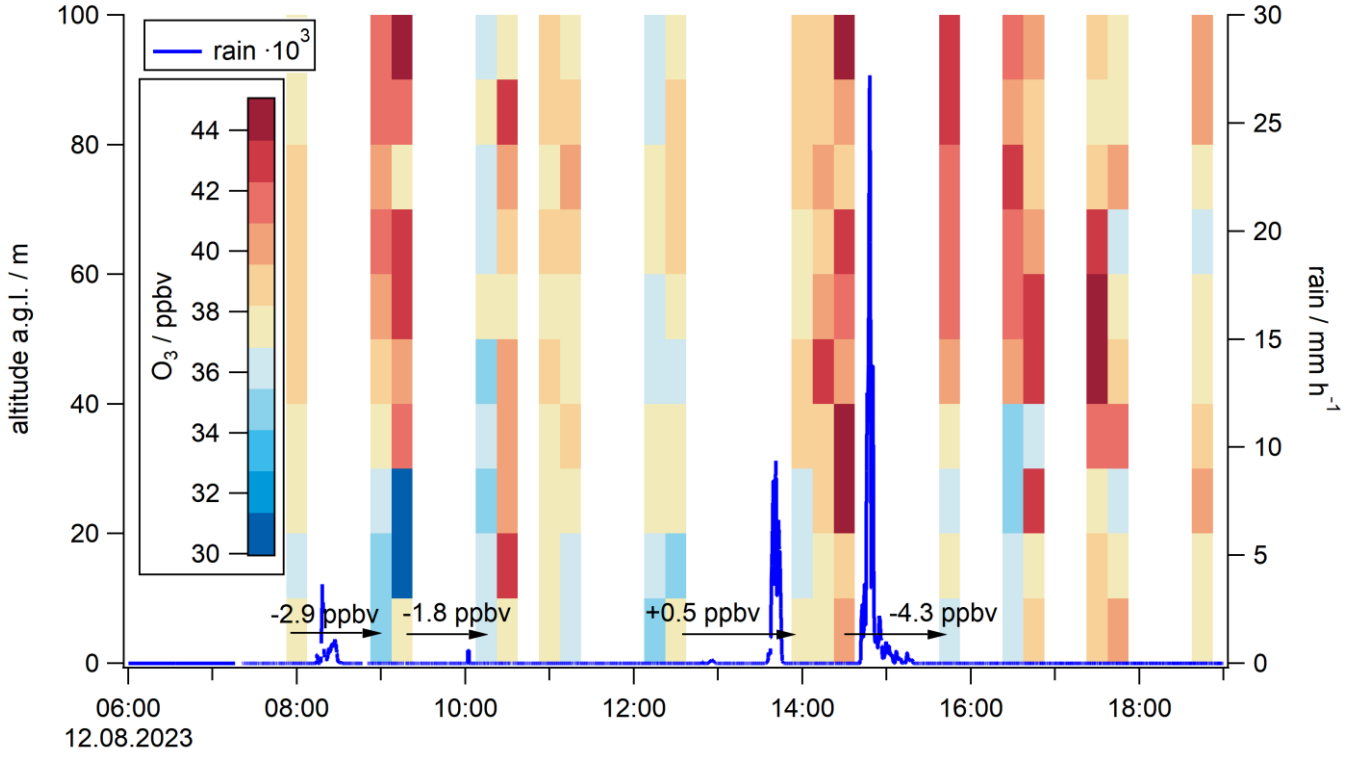

Figure S15: A vertically resolved O_3-time series (15 minute-time increments with a 5 m altitude range, color-scaled, measured with FLab) show a decrease of 3.0 ± 1.3 ppbv O_3 at the lowest bin after rain (blue, 1 s data) and slow increase as O_3-rich air is injected from higher levels.

References

Stein, A. F., Draxler, R. R., Rolph, G. D., Stunder, B. J. B., Cohen, M. D., and Ngan, F.: NOAA's HYSPLIT Atmospheric Transport and Dispersion Modeling System, Bulletin of the American Meteorological Society, 96, 2059-2077, 10.1175/bams-d-14-00110.1, 2015.